Stabilization of the Kerr effect by self-induced ionization: Formation of optical light spatially localized structures

Thierry Lehner and Nicole Auby*
Laboratoire de Physique des Milieux Ionisés (PMI), CNRS UMR No. 7648, Ecole Polytechnique, 91128 Palaiseau Cedex, France
(Received 12 July 1999)

The nonlinear propagation of ultrashort laser pulses launched into the air is investigated. The formation of optical light ''bullets,'' or spatially localized structures, has been experimentally observed recently. Their stability is shown as due to the occurrence of a dynamical balance between two opposite nonlinear effects: an optical focusing Kerr effect balanced by a defocusing self-induced multiphoton partial ionization of the neutral gas. Characteristics of the ''bullets'' are predicted analytically and confirmed numerically. They are found to be in agreement with observations.

PACS number(s): 42.65.Tg, 42.65.Jx, 52.35.Mw, 51.70.+f

I. INTRODUCTION

Nonlinear propagation of intense laser radiation through transparent media can generate interesting effects. One of them is the well-known Kerr self-focusing effect leading to a spatial collapse of the laser beam within a finite self-focusing distance (hereafter noted L_{sf}). A new situation occurs when the cancellation of opposite nonlinear effects may allow a stable propagation over large distances even when the incident laser pulse power is well above the critical one for the Kerr self-focusing (P_c). Indeed, the formation of so-called optical light ''bullets'' (in the sense of spatially localized structures and not spatio-temporal solitons) has been observed recently in experiments [1–3]. In these measurements well-collimated powerful femtosecond laser pulses were fired into the air and were found to collapse into radially finite ''filaments'' that self-propagate, keeping a stable shape over dozens of meters. In another experiment [4] a light beam was focused into a chamber filled with gas, but there filamentation of the laser beam was occurring, preventing it from a stable propagation.

In this paper the stability of the bullets is explained with the help of a simple nonlinear propagation model for the light beam. Recent numerical simulations have been performed yielding features close to our conclusions [5], whereas an alternative model using a moving focus has been put forward [6].

The beam propagation is considered within two separate areas. In a first region only the Kerr effect exists with a spatial collapse of the beam radius and self-phase modulations (SPM's). In a second region the beam intensity is sufficient to ionize the air and a plasma is created able to defocus the beam and adding a new component to the refractive index. It is shown, as was noted previously in [1], that the dynamical equilibrium between these two opposite nonlinearities leads to the observed spatially stable channels.

*Also at Service de Recherche sur les Surfaces et Irradiation de la Matière (SRSIM), Centre d'Etudes Nucléaires de Saclay, 91190 Gif-sur-Yvette Cedex, France.

II. THE EXPERIMENTAL DATA

Let us first summarize typical experimental features: we shall use the experimental figures of the LOA group partially published in [2,12] in the following.

The laser facility consists of an optical laser Ti:Sa chain delivering ultrashort pulses ($\tau<150$ fs) with a moderate energy (30 mJ), a repetition rate of 20 Hz at a wavelength λ of 800 nm. Here the pulse beam is merely fired into a long corridor without any lensing system, its initial radius r_i being about 1 cm. The beam begins first to exhibit self-phase modulation (SPM) and radius shrinking typical of a spatial collapse due to the self-focusing Kerr effect. The beam radius goes down to around 100 μm after about 10 m. Note that for short pulses the initial power P_i could easily overcome the Kerr critical power P_c. However, the SPM develops preferentially in the red side of the laser spectrum and a continuous self-frequency redshifting (SFS) is also seen saturating after a propagation distance of 12–15 m. In a second region the formation of a light beam of narrow radial size is observed and found to be stable over a distance of 30–50 m. The spectrum and intensity (I_f) in this ''filament'' are then clamped to their value at the location of the filament onset. There is no additional averaged blue SFS due to an ionization front, but now a preferential SPM is present on the blue side of the spectrum as compared to the spectrum observed in the first Kerr region.

Typical data are (a) recorded spectra taken at different spatial locations (radially integrated over filament size), (b) temporal autocorrelation trace, and (c) energy measurements. In the filament the energy E_f is found to be about 0.7–1 mJ, while the radial size r_f is about 100–150 μm. There is no measured temporal compression inside the filament (within the radial and time resolutions).

III. THE NONLINEAR PROPAGATION EQUATION

To explain the experimental features, we intoduce a nonlinear propagation equation. We start from the Maxwell equation for the electric field E of the pulse written as

$$(\Delta-\partial_{t^2}^2/c^2)(n_0+\delta n)^2\overline{E}(\overline{r},t)=\overline{0}, \tag{1}$$

where n_0 is the unperturbed refractive index of the medium and δn the perturbed one which can depend on the nonlinearly of E. We assume that an envelope approximation is valid for a pulse with a long duration with respect to the time optical period and a typical spatial variation of the pulse electric field longer than the optical wavelength. We split E into amplitude u and phase Φ, as $\overline{E}=\overline{u}e^{i\phi}$, and we average Eq. (1) over the fast phase ϕ chosen as $\phi=kz-\omega t$. We get a model equation of the nonlinear Schrödinger type for the slowly varying complex amplitude $\overline{u}(\overline{r},t)$ as

$$[(2ik\partial_z+\Delta_\perp)+g(|u|^2)]\overline{u}(\overline{r},\zeta)=\overline{0},$$

$$g\approx 2k^2[\delta n(|u|^2/n_0)]. \tag{2}$$

We have neglected terms in $(\delta n)^2$ in Eq. (1) and have changed the time variable t into $\zeta=t-z/V_g$, the propagation variable along the pulse, V_g being the pulse group velocity. The envelope approximation for u remains valid even for short pulses (but generally longer than 100 fs), and at moderate intensities (below a few 10^{14} W/cm^2) [7], these conditions are satisfied here.

We wish to explain what has been observed using a minimal and simple theory. For this purpose we shall drop all the nonlinear terms that appear to be irrelevant in the analysis.

Hence in Eq. (2) we also neglect higher-order time derivatives such as $\beta_2\partial^2_{\zeta^2}$ and $\beta_3\partial^3_{\zeta^3}$, respectively, connected with pulse time compression and pulse broadening (since none of them are observed) by group velocity dispersion (this point will be discussed later). Also crossed time and spatial derivatives are discarded and as well the self-steepening process bringing another contribution proportional to $-\partial_\zeta((uu^*)u)$.

Equation (2) has three terms: the first one describes the propagation, the second accounts for possible diffraction, and the last term holds the two relevant nonlinearities, here the competiting Kerr effect and the plasma ionization process.

A. General considerations

There is no available general theoretical tool to analyze Eq. (2) exactly. However, to proceed analytically we can split u itself into a slow modulus and phase assuming an initial radial symmetry of the pulse:

$$\overline{u}(\overline{r},\zeta)=\hat{e}u(\overline{r},\zeta)e^{i\Phi_{\rm NL}(\overline{r},\zeta)}.$$

$$\overline{r}=(r,z).$$

The recorded spectra (J) are the main observed data and the nonlinear phase factor $\Phi_{\rm NL}$ is one important quantity to describe them.

The spectrum J_ω is defined by

$$J_\omega(r,z)=\left|\int_{-\infty}^{+\infty}u(r,z,\zeta)e^{i[(\omega-\omega_0)\zeta+\Phi_{\rm NL}(r,z,\zeta)]}d\zeta\right|^2, \tag{3a}$$

$$J_\omega(z)=\int d^2r\,J_\omega(r,z)R(r-r^*). \tag{3b}$$

J_ω could be radially integrated as in Eq. (3b) with a given convolution profile R to account for finite experimental resolution.

To gain more insight into the phase behavior, we shall use two simple analytic methods. First, we may integrate directly Eq. (2), neglecting the diffraction, and this yields at once

$$\partial_z|u|=0,$$

$$\Phi_{\rm NL}(r,z,\zeta)=-\int_0^z g(|u|^2)dz/2k. \tag{4}$$

Thus we get a modulus constant in z and a phase increasing linearly with distance, apart from their dependence in r and ζ that are given by the initial conditions for $|u|$. We shall suppose here that g is a real function.

As a second method we use the radial paraxial approximation. We recall that it consists of analyzing the evolution of the phase and radius of the electric field along z within the core of the beam. Thus we make a radial expansion into the assumed small parameter (r/r_i), r_i being the initial beam radius at $z=0$. The validity of the method requires clearly to stay in the core of the beam. By this technique we reduce the initial partial differential equation (PDE) into two coupled ordinary differential equations (ODE's). Taking the real and imaginary parts of Eq. (2), these equations are found to be

$$k\partial_z|u|^2=-[\Delta_{rr}\Phi_{\rm NL}+{\rm Im}(g)]|u|^2-(\partial_r\Phi_{\rm NL})\partial_r|u|^2, \tag{5a}$$

$$2k\partial_z\Phi_{\rm NL}={\rm Re}(g)+\Delta_{rr}|u|^2/|u|-(\partial_r\Phi_{\rm NL})^2. \tag{5b}$$

Now because of diffraction and possible dissipation, u will also depend on z through the radial derivatives.

Using a radial Gaussian trial function as a starting ansatz and expanding the phase to second order in $(r/r_i)=r$, we introduce three auxiliary functions f, φ, and χ as

$$u(r,z,\zeta)=[u_0(\zeta)/f(z,\zeta)]e^{-(r/r_0f)^2/2}e^{i\Phi_{\rm NL}(r,z,\zeta)}, \tag{6}$$

$$\Phi_{\rm NL}(r,z,\zeta)=\varphi_{\rm NL}(z,\zeta)+(r^2/2)\chi(z,\zeta)+\vartheta(r^4), \tag{7}$$

$$\chi(z,\zeta)=f'_z/f. \tag{8}$$

Expression (6) is a solution of Eq. (4) for uu^*, while relation (8) is obtained by inserting Eq. (7) into Eq. (4). Next, by equating the coefficients of zeroth- and second-order terms in the r expansion in both members of Eq. (5) using expression (6) in g itself expanded in r, we obtain two coupled ordinary equations for f and φ as

$$(2k)f''_{z^2}/f=1/(r_i^3f^4)-{\rm Re}(g)|_{r^2}, \tag{9}$$

$$(2k)\varphi'_{(nl)z}=-2/(r_i^2f^2)-{\rm Re}(g)|_0. \tag{10}$$

With the choice of three initial conditions for f, f', and for Φ at the boundary $z=0$, we can follow the evolution of the radius and phase in the core of the beam along z.

The paraxial approximation applies also to simpler equations describing mere diffraction in a vacuum, allowing one to recover the usual Rayleigh diffraction laws (linear problem). Normalizing the variables $r'=r/r_i$, $z'=z/z_r=2kr_i^2$,

$w_i = 2r_i$, z_r being the Rayleigh length ($\pi w_i^2/\lambda$), and by setting $g=0$ in Eqs. (9) and (10) with the initial conditions $f(z=0)=1$, $f'(z=0)=0$ (parallel beam), and $\Phi(z=0)=0$, we find the familiar expressions for a naturally diverging Gaussian beam as

$$f''=1/f^3, \quad \varphi' = -2/f^2,$$

$$f=[1+(z/z_r)^2]^{1/2}, \quad \Phi=\arctan(z/z_r).$$

In this case the initial spectrum is unchanged with distance, but the radius and phase evolved with z. For small distances Φ varies linearly with z and then saturates.

Now we shall examine the case of the two involved ''nonlinearities,'' first separately and then together.

B. Kerr region

It is defined as the region of negligible ionization, i.e., of vanishing plasma corrections to the refractive index.

1. Instantaneous Kerr effect

We rewrite Eq. (2) as

$$(2ik\partial_z + \Delta_\perp + 2k^2(n_2 I))u(\overline{r},\zeta)=0. \tag{11}$$

The usual nonlinear index n_2 is introduced in Eq. (11), and we need the precise value of n_2 to compute the L_{sf} distance. By phase retrieval techniques [8] applied to the recorded spectra (see also [9] for air) and using Eq. (3), one gets a good determination of the index as $n_2 = 3\times 10^{-19}\,\mathrm{cm^2/W}$. The Kerr critical power P_c enters as a normalizing factor of the nonlinear term in Eq. (11) as

$$P_c = \lambda^2/(2\pi n_2), \tag{12}$$

$$P_c/4 = (\varepsilon_0 c)u_c^2 S = I_c S, \quad S=\pi r_1^2, \quad \text{with } u'=u/u_c,$$

$$I=(\varepsilon_0 c)uu^*,$$

$$(i\partial_{z'} + \Delta_{\perp'}) + [P(|u'|^2)/(P_c/4)]\overline{u}'(\overline{r},\zeta)=0. \tag{11'}$$

Here the initial experimental power was $P_i = (30\ \mathrm{mJ}/150\ \mathrm{fs}) = 200\ \mathrm{GW} \gg P_c = 3.4\ \mathrm{GW}$ [from Eq. (12) for $\lambda = 0.8$ nm and n_2 is given above]. Thus an initial radial spatial collapse is expected systematically for short enough pulses. The Kerr nonlinear phase reads from Eq. (4)

$$\Phi_{NL}^K(r,z,\zeta) = k\int_0^z n_2(r,z',\zeta)I(r,z',\zeta)dz'. \tag{13a}$$

If the amplitude u were to remain constant in z (i.e., neglecting diffraction effects), we would recover a phase varying linearly with z as

$$\Phi_{NL} = (z/z_r)(P_i/(P_c/4)) \tag{13b}$$

and so would vary the instantaneous frequency shift (ISF) defined by

$$\Delta\omega(r,z,\zeta) = -\partial_\zeta \Phi_{NL}. \tag{14}$$

The phase is modulated since P_i is a function of ζ, and we choose *a priori* (aside from a small chirp in time defined by the parameter C) a symetrical initial experimental profile with a double Gaussian shape in r and ζ as

$$u(r,z=0,\zeta) = u_0 e^{-(r/r_0)^{2/2}} e^{-(\zeta/r)^2(1+iC)/2}. \tag{15}$$

We see that the frequency shift $\Delta\omega$ would be an antisymetrical function of ζ, thus bringing as much redshift (and SPM) in the rising front as blueshift in the trailing edge of the pulse, with a zero self-frequency shift (SFS) $\langle\Delta\omega\rangle$ averaged over ζ. If diffraction is included, the analytic dependence in z is more difficult to find, but progress can be made using the paraxial method. Applying the paraxial approximations to Eqs. (11) and (11′), we are left with the two coupled ordinary equations

$$\partial^2_{z'^2} f(z,\zeta) = [1-b^2(\zeta)]/f^3, \tag{16a}$$

$$\partial_{z'}\Phi(z,\zeta) = [-2/f^2 + b^2(\zeta)]/f^2, \tag{16b}$$

$$b(\zeta) = u_i(r=0,z=0,\zeta)/u_c.$$

We recover the power threshold $P=P_c/4$ ($b=1$) by setting $f''=0$. With our given initial conditions ($f=0$, $f'=1$, $\Phi=0$), we can easily integrate Eqs. (16a) and (16b):

$$f=\{1\pm[z/L_{sf}(\zeta)]^2\}^{1/2}, \tag{17}$$

$$\mathrm{sgn}+ \text{ for } b<1, \quad \mathrm{sgn}- \text{ for } b>1,$$

$$\Phi = L_{sf}(\zeta)[-2+b^2(\zeta)]\arg\tanh[z/L_{sf}(\zeta)] \quad \text{for } b>1, \tag{18a}$$

$$\Phi = L_{sf}(\zeta)[-2+b^2(\zeta)]\arctan[z/L_{sf}(\zeta)] \quad \text{for } b<1, \tag{18b}$$

$$L_{sf}(\zeta) = z_r/[|1-b^2(\zeta)|]^{1/2}. \tag{19}$$

L_{sf} is predicted by relation (19). The 1 in the argument of the denominator of Eq. (19) accounts for diffraction and is negligible for $P_i/P_c \gg 1$. Numerically, at the top of the pulse we find for $r_i = 0.5$ cm a value $L_{sf} = 19$ m to be compared with the observed value around 12–15 m for the collapse of the beam to a finite radius. Thus at this stage SPM and radial collapse are recovered as the usual features of a Kerr effect.

2. Noninstantaneous Kerr effect

However, the experiments show a preferential SPM in the red part of the spectrum, showing an asymmetry with a nonzero averaged SFS $\langle\Delta\omega\rangle$. But this shift is saturating in z around L_{sf} with a maximum value of $\langle\Delta\omega\rangle/\omega = -\delta\lambda/\lambda = -10/800 = -1.25\%$. The introduction of a noninstantaneous Kerr effect brings an explanation. We shall consider now a modified propagation equation as

$$[2ik\partial_z + \Delta_\perp + 2k^2 n_2(I)]u(\overline{r},\zeta)=0, \tag{20}$$

$$(\partial_\zeta + 1/\tau_2)n_2(\overline{r},\zeta) = n_{20}I(\overline{r},\zeta)/\tau_2. \tag{21}$$

A new parameter appears as $y=(\tau/2\tau_2)$, the ratio of pulse duration to the relaxation constant τ_2. Setting $\tau_2=0$ allows us to recover the previous model. The finite τ_2 corresponds to a finite time answer for molecular polarization reorientation after excitation by the pulse. It could be shown that the

two times τ and τ_2 are of the same order (here around 100 fs) [9,10]. This last result could be obtained by estimating the rotational constant and the kinetic momenta of the populated molecular states. Such a ''Raman'' effect describes the relaxation of the polarization of the air diatomic molecules populated by the light pulse into excited electronic and rotational states. Note that for mononuclear diatomic molecules such as N_2 and O_2 in air the Raman effect involves necessarily two photons for parity conservation reasons. A formal solution to Eq. (21) for the index $n_2(I)$ is then given by

$$n_2(I)(r,z,\zeta)=(n_{20}/\tau_2)\int_{-\infty}^{t} e^{-(\zeta-\zeta')/\tau_2} I(r,z,\zeta')d\zeta', \tag{22}$$

so that Eq. (20) becomes a nonlinear integrodifferential equation as

$$\left(2ik\partial_z+\Delta_\perp+2k^2\frac{n_{20}}{\tau_2}\times\int_{-\infty}^{t} e^{-(\zeta-\zeta')/\tau_2} I(r,z,\zeta')d\zeta'\right)u(r,z,\zeta)=0. \tag{23}$$

We analyze again the phase $\Phi_{\rm NL}$, taking the same initial profile given by Eq. (15) without the temporal chirp $C=0$. We see that Φ is an asymmetrical function of time bringing more SPM in the red side of the spectrum. The IFS is now globally ''redder'' than ''bluer'' with a nonzero averaged red SFS

$$\langle\delta\omega(r,z)\rangle=1/\tau\int_{-r/2}^{r/2}\Delta\omega(r,z,\zeta)d\zeta =-[\Phi_{\rm NL}(r,z,\tau/2)-\Phi_{\rm NL}(r,z,-\tau/2)]/\tau, \tag{24a}$$

$$\langle\Delta\omega\rangle/\omega=(1/2\pi)(4P_0/P_c)(\lambda/c\tau)\langle g_K(x,y)\rangle(z/z_r), \tag{24b}$$

$$\langle g_K(x,y)\rangle=-[g_1(1/2,y)-g_1(-1/2,y)],$$

$$x=\zeta/\tau,\quad y=\tau/2\tau_2, \tag{25}$$

$$g_1(x,y)=2y\int_{-\infty}^{x} b^2(x')e^{-2y(x-x')}dx'.$$

For $z=L_{\rm sf}$ given by Eq. (19), we can predict a SFS depending on the pulse power in $P^{1/2}$ for $P_i/P_c\gg 1$ since we have

$$\langle\Delta\omega_1\rangle/\omega=(1/2\pi)(4P_0/P_c)^{1/2}(\lambda/c\tau)\langle g_K(x,y)\rangle. \tag{26}$$

Using the profile (15), we get for the function g_1

$$g_1(x,y)=ye^{y^2/4-2xy}\pi^{1/2}[1+\mathrm{erf}(x-y)]. \tag{25'}$$

For y around 1/2 with $P_i/P_c=60$, $L_{\rm sf}=19$ m for $w_i=1$ cm, and $z_r=392$ m, we get $\langle\Delta\omega\rangle/\omega=-1.41\%$, in good accordance with the observation $[\langle g\rangle=-(0.37/2)(\pi)^{1/2}]$. In fact, one has to recompute the $L_{\rm sf}$ value; see the paraxial section below. A radial integration affects poorly the value $\langle\Delta\omega\rangle$, but may alter significantly the spectrum since the phase factor varies rapidly and phase mixing could occur.

3. Paraxial analysis of the noninstantaneous Kerr effect

Starting from Eq. (23), we derive two coupled evolution equations for the beam radius $f=[r(z,\zeta)/r_i]$ and phase Φ that are now ordinary integro-differential equations as

$$\partial^2_{z'^2}f(z',\zeta)=4\left[1/f^3(z',\zeta)-[f(z',\zeta)/\tau_2]\times\left(\int_{-\infty}^{\zeta}[b^2(\zeta')/f^4(z',\zeta')]e^{-(\zeta-\zeta')/\tau_2}d\zeta'\right]\right), \tag{27}$$

$$\partial_{z'}\Phi(z',\zeta)=-2/f^2+(1/\tau_2)\int_{-\infty}^{\zeta}[b^2(\zeta')/f^2]e^{-(\zeta-\zeta')/\tau_2}d\zeta'. \tag{28}$$

If the ζ variation of f is comparable to the exponential term or if f cannot be factorized as a product of a function of z and of a function of ζ, then we do need a numerical integration to solve Eqs. (27) and (28). By using a simple Runge-Kutta fourth-order algorithm, we find that f varies more slowley than the exponential term and it can be taken out of the integral in ζ'. However, this result is true only for small values of the propagation distance z: afterwards, f varies quickly in time and cannot be taken out of the integral. We are back to a system such as Eqs. (16a) and (16b) with solutions like Eqs. (17) and (18) modified by substituting for the function b a new function B defined by $B^2=g_1$. The self-focusing length $L_{\rm sf}$ is modified as well, since now

$$L_{\rm sf}^{(')}(\zeta)=z_r/[|1-B^2(\zeta)|]^{1/2}. \tag{19'}$$

Also, the power threshold in the paraxial analysis is modified by the condition $B=1$ instead of $b=1$ (for $P=P_c/4$).

Using again the profile (15), we get a value $g_1(0)=1.4$ [see Eq. (25')] and the minimum $L_{\rm sf}$ value is now 16 m instead of 19 m. The reduced radius f hence varies according to Eq. (18), but it is modified by using Eq. (25'): thus, f varies more slowly than the exponential term in ζ.

The self-frequency shift computed by Eq. (26) should also be corrected as follows:

$$\langle\Delta\omega\rangle/\omega\approx(1/2\pi)(4P_0/P_r)^{1/2}(\lambda/c\tau)\langle g_K(x,y)\rangle[1/g_1(0)]^{1/2}. \tag{29}$$

Numerically, the relative SFS is $\langle\Delta\omega/\omega\rangle=-1.19\%$, closer than the previous one to the observed value. This is remarkable since y is not known with an accurate precision and we have used a rather crude model.

It is interesting to compare the phase and frequency shifts (IFS,SFS) given by the qualitative method and by the paraxial ones.

By using the new phase Φ as,

$$\Phi=[L_{\rm sf}(\zeta)/z_r][-2+B^2(\zeta)]\mathrm{arctanh}[z/L_{\rm sf}(\zeta)]\quad\text{for } B>1, \tag{30}$$

the qualitative phase given by Eq. (13b) is recovered from Eq. (30) as for small z, $\Phi \approx z'[-2+B^2(\zeta)]$, while without diffraction $\Phi \approx z' B^2(\zeta)$.

Note that even without any diffraction effect in Φ and in L_{sf} the phase is now diverging at $z=L_{\mathrm{sf}}$ like $\operatorname{arctanh}(z/L_{\mathrm{sf}})$ as in the paraxial instantaneous Kerr case. The more complete IFS and SFS expressions are now given by

$$\Delta\omega = -\partial_{\zeta}(B^2)(L_{\mathrm{sf}}/z_r)\operatorname{arctanh}[z/L_{\mathrm{sf}}(\zeta)] + (\delta\Delta\omega), \tag{31a}$$

$$(\delta\Delta\omega) = (-2+B^2)[-\partial_{\zeta}(L_{\mathrm{sf}}/z_r)][\operatorname{arctanh}(z/L_{\mathrm{sf}})(\zeta)] - (z/L_{\mathrm{sf}})/[1-(z/L_{\mathrm{sf}})^2]. \tag{31b}$$

In Eqs. (31), for B even, L_{sf} is also even and the first term of the right-hand side that gives again the IFS in the qualitative analysis has a nonzero averaged SFS. Note the appearance of a singularity at $z=L_{\mathrm{sf}}$ now of the radius, but also of the frequency shift in this paraxial approximation. The SFS vanishes for B^2 even, and it is given by, with the help of Eq. (30),

$$\langle\Delta\omega\rangle/\omega = (\langle\Delta\omega\rangle/\omega)(-1/2) - [(\langle\Delta\omega\rangle/\omega)(1/2)], \tag{32}$$

$$(\langle\Delta\omega\rangle/\omega)(1/2) = (1/\omega\tau)[L_{\mathrm{sf}}(1/2)/z_r] \times [-2+B^2(1/2)]\operatorname{arctanh}[z/L_{\mathrm{sf}}(1/2)],$$

$$(\langle\Delta\omega\rangle/\omega) = 0 \text{ for } B^2 \text{ even}.$$

With the choice of Eq. (15) for u, B^2 is asymmetric and Eq. (32) is diverging at $z=L_{\mathrm{sf}}$. Also, the intensity I that scales like $1/f^2$ diverges at $z=L_{\mathrm{sf}}$: however, this divergence is removed by a finite radial integration since Eq. (6) for u is power conservative. This kind of singularity looks similar to the one encountered in the approach of the blowup in a theoretical analysis of the nonlinear Schrödinger equation.

We can conclude that within our simple model the intensity profile at the center of the beam ($r=0$) has an ''amplification factor'' of the form

$$I_0(r=0,z,\zeta) = I_0(r=0,z=0,t)/[1-(z'/L'_{\mathrm{sf}}(z',\zeta))^2].$$

Note that just prior and close to the L_{sf} distance we are at the filament onset because the energy density becomes strong enough to produce sufficient ionization of the surrounding air.

C. Ionization region

To describe the plasma creation, we need first an ionization model, but computation of the multiphotoionization cross section, even for diatomic molecules, with the absorption of several photons is a very hard task. We have designed the following trick to get an order of magnitude of the cross section: we connect the Keldysh formula for ionization with a ''modern'' preexponential factor [11] to describe tunneling ionization at high flux with a multiphotonic formula at low flux, washing out the details of eventual atomic resonances. Close scrutiny of numerous multiphoton experiments teaches us that a good flux to connect both processes could be taken around 10^{14} W/cm^2. We consider a single ionization probability W and photoionization only. At higher flux (here the initial flux is $I=6\times10^{10}$ W/cm^2 and the ionization is very weak), multiple ionization can occur, whereas recombination is negligible in cold plasmas in such short times and at moderate densities. The only other possible ionization mechanism (there is no breakdown in the gas on this too short time scale) could be by electron impact ionization (primary electrons could produce secondary electrons by ionizing collisions). But since cross sections are around 10^{-16} cm^2 at a maximum pulse energy in N_2 and O_2 for electron impact, one can verify that, at low flux and moderate pressure, the ionization time is much longer than the pulse duration. Hence the photoionization process is by far the leading ionization mechanism here.

We use a notation designed for high intensity, q being an interaction parameter ratio of the pulse electric field normalized to the Compton electric field E_{ct} (with a Compton intensity I_{ct}), and we write the ionization probabilities W_1 and W_2 as

$$W_1 = \sigma_p I^p, \tag{33a}$$

$$p = \mathrm{Int}(h\nu/E_a),$$

$$W_2 = a q^{1/2} e^{-d/q}, \tag{33b}$$

$$q = (I/I_{ct})^{1/2}, \quad a = 4.2^{3/2} p (E_a/\hbar) S^{1/2}/e,$$

$$d = 2^{3/2}/3pS^{1/2}, \quad S = (E_a/m_e c^2), \quad I_{ct} = \varepsilon_0 E_{ct}^2,$$

$$E_{ct} = m_e c \omega_0 / e.$$

The number of ionizing photons is $p=10$ and 8, respectively, for N_2 and O_2 with respective first ionization potential E_a around 15.6 and 12 eV since the incoming red photons have an energy of 1.55 eV. To simplify, we assume a ''mean molecule'' with the air mass and choose a mean value of $p=9$ with $E_a=12$ eV (because O_2 is preferentially ionized) and get a practical formula for the multiphoton ionization probability W_1 at low flux as $W_1 = A(I/I_s)^9$, $I_s = 10^{14}$ W/cm^2 with $A=0.1/\tau$. Defining a mean ionization rate by

$$\alpha = W\tau \tag{34}$$

we get an ionization of the order of 10% for a laser flux equal to I_s.

The equation of the single ionization generating free electrons with a density N_e is simply given by (N_0 being the density of neutrals)

$$\partial_{\zeta} N_e(\overline{r},\zeta) = N_0 W(\overline{r},\zeta), \tag{35}$$

$$N_e(r,z,\zeta)/N_0 = 1 - \exp\left(- \int_{-\infty}^{t} W(r,z,\zeta')d\zeta' \right), \tag{36a}$$

$$N_e/N_0 \approx \int_{-\infty}^{t} W(r,z,\zeta')d\zeta'. \tag{36b}$$

We shall suppose that only weak ionization occurs and shall use Eq. (36b) later on only.

D. Spectral plasma blueshift due to the ionization front

The free electrons liberated by the ionization process generate a plasma and add a contribution to the refractive index δn_p to be compared to the Kerr contribution from neutrals. This index reads

$$\delta n_p(\overline{r},\zeta) = \{1 - (\omega_{pn}^2/\omega^2)[N_e(\overline{r},\zeta)/N_0]\}^{1/2}, \tag{37a}$$

$$\delta n_p(\overline{r},\zeta) \approx -(\omega_{pn}^2/2\omega^2)[N_e(\overline{r},\zeta)/N_0], \tag{37b}$$

$$\omega_{pn}^2 = N_0 e^2/m_{0e}\epsilon_0 .$$

The index variation δn_p is a nonlinear function of intensity through Eqs. (33)–(37), ω_{pn} being the plasma frequency normalized to the neutral density, and we have supposed both a weak ionization and an underdense plasma (air is transparent for the wavelength of the incoming infrared light) so that we can make the approximation

$$(\omega_{pe}^2/\omega^2) = (N_e/N_0)(\omega_{pn}^2/2\omega^2) \ll 1.$$

Due to the refractive index δn_p, a finite IFS appears, which is given by

$$\Delta\omega_P(r,z,\zeta) = -\partial_\zeta \Phi_{\mathrm{NL}}^p = -k\partial_\zeta \int_0^z \delta n_p(r,z',\zeta)dz', \tag{38a}$$

$$\Delta\omega_P = (k/2)(\omega_{pn}/\omega)^2 \partial_\zeta \int_0^z \int_{-\infty}^{\zeta} W(r,z',\zeta')d\zeta' dz',$$

$$\Delta\omega_P/\omega = (\omega_{pn}/\omega)^2/(2c\tau)\int_0^z \tau W(r,z',\zeta)dz', \tag{38b}$$

$$\int_0^z \tau W dz' \approx \alpha z.$$

We expect again a low ionization rate. We see in Eq. (38b) that unlike the Kerr effect inducing blue or red SPM depending on the temporal loaction within the pulse (front or back), the plasma brings only positive, i.e., blue, SPM contributions (since W is positive) with a nonzero averaged SFS. This SPM is effectively observed in experiments when the filament is created since the blue SPM of the spectrum is noticeably increased ([2,12]).

We find this SFS by averaging over ζ and using the qualitative phase, disregarding diffraction:

$$\langle \Delta\omega_p \rangle/\omega = (z/2c\tau)(\omega_{pn}/\omega)^2(\tau\sigma_p I_c^p/4^p)\langle g_p \rangle, \tag{39a}$$

$$\langle g_p \rangle = \int_{-1/2}^{-1/2} b^{2p}(x')dx'. \tag{39b}$$

The integral in Eq. (39b) is evaluated by setting condition (15) as $\langle g_p \rangle = \frac{1}{2}(\pi/p)^{1/2}\,\mathrm{erf}(p^{1/2}) \approx \frac{1}{2}(\pi/p)^{1/2}$ for high p ($p=9$). Numerically, for $P=1$ atm, $N_0 = 3\times 10^{19}\,\mathrm{cm}^{-3}$ a huge relative averaged blueshift of the order of 20%/cm is expected by predicting a value of the ionization rate α of the order of 10^{-3}. However, such a blueshift is not observed in the experiment under study. But we have completely ignored the Kerr effect in this section.

E. Simultaneous Kerr and ionization effects

1. Propagation equation

In the region where both nonlinear effects occur, the complete envelope propagation equation should be considered, by adding the corresponding refractive indexes as

$$\{2ik\partial_z + \Delta_2 + 2k^2[n_2'(I) + \delta n_p(I)]\}u(\overline{r},\zeta) = 0, \tag{40}$$

$$n_2'(I) = n_2(I)[1 - N_e(I)/N_0].$$

More explicitly, the new equation for the u evolution is

$$\left\{ \begin{array}{l} 2ik\partial_z + \Delta_2 + 2k^2\left((n_{20}/\tau_2)\int_{-\infty}^{\zeta} I(r,z,\zeta')e^{-(\zeta-\zeta')/\tau_2}d\zeta' \right)\left(1 - \sigma_p\tau\int_{-\infty}^{\zeta} I^p(r,z,\zeta')d\zeta' \right)\cdots \\ \cdots - \left((\omega_{pn}/\omega)^2(1/2)\sigma_p\tau\int_{-\infty}^{\zeta} I^p(r,z,\zeta')dz' \right) \end{array} \right\} u(r,z,\zeta) = 0. \tag{41}$$

Here, in fact, the neutral depletion will be weak and will be neglected in the Kerr term since ionization will always remain at a very low level.

We see that the opposite sign of the two refractive indexes allows the stabilization of the *a priori* spatial Kerr collapse when these indexes reach the same magnitude. This point is confirmed by the experiments, but also by numerical studies solving the complete EDP's like Eqs. (40) and (41) where solitary wave structures are found and are observed to remain stable in the course of their propagation [5,13]. Also,

since the group velocities in air and plasma are equal and opposite in this case, possible pulse broadening effects due to group velocity dispersion (GVD) are canceled.

2. "Bullet" characteristics

To determine the filament equilibrium, in the radial core of the pulse, which is dynamical balance for ionization, which is itself a dynamical process, we write the effective equality of the nonlinear refractive indexes n_2 and δn_p at a given z on average over ζ. This procedure provides an equation for determining I_f, the energy density in the channel. We find the following results, by assuming a cylindrical beam:

$$\langle n_2(I)\rangle = \langle \delta n_p(I) + n_d\rangle, \qquad n_d \approx [1.22\lambda/w_i(z)]^2/8\pi, \tag{42}$$

$$I_{f0} = \{[\langle g_k(x,y)\rangle/\langle g_p(x)\rangle](1/4n_2)(\omega/\omega_{pn})^2(1/\sigma_p\tau)\}^{1/(p-1)}, \tag{43}$$

$$I_{f0} \approx I_s\{(I_s/I_c)[\langle g_k\rangle/(\langle g_p\rangle 2\times 10^{-1})] \times(\lambda/\pi r_i)^2(\omega/\omega_{pn})^2\}^{1/(p-1)}. \tag{44}$$

We shall further neglect the diffraction contribution n_d. In Eq. (44) we have used the result of Eq. (33a), with $p=9$, and the definition (15). We then compute the averaged values for g_k and g_p from Eqs. (25′) and (39b) with $y=1/2$. We find a numerical value of I_f as $I_f = 6-7\times 10^{13}$ W/cm^2. Using our ionization model, we deduce an ionization rate of $\alpha = 1-2\times 10^{-3}$, due to the factor $(I_f/I_s)^9$. Numerical simulations have confirmed this value of the ionization rate [5].

The dynamics of ionization is very important for short pulses because it determines through its nonlinear (instantaneous) intensity dependence the dynamic of the filament. Instead, for longer pulses at higher fluxes such as those used for studies of relativistic self-focusing (RSF), the ionization is instantaneous and there is no need to include the ionization dynamics in the pulse propagation except for a specific treatment of ionization fronts.

A quick estimate of the filament radius r_f could be obtained from our knowledge of RSF [14] since the beam radius could not be smaller than the skin depth defined by

$$\lambda_d = c/\omega_{pe} = (c/\omega_{pn}\alpha^{1/2}). \tag{45}$$

Knowing I_f by Eq. (44), we get $\lambda_d = 70\,\mu$m, not very far from the observed filament radius.

To finish this part we note that the equality of the averaged indexes in the filament implies also an exact cancellation of the corresponding self-frequency shifts (SFS's) by definition. Thus there is a frequency shift clamping when the balance of indexes is achieved and the intensity remains also fixed. This explained why no additional SFS's are observed after the filament onset. In particular, there is no additional averaged blueshift due to the ionization. However, even with equality on the average the instantaneous IFS's do not compensate each other, and thanks to the different power laws in I^P for n_p and in I for n_2, we have roughly the relationship for IFS's: $\Delta\omega_p = -p\Delta\omega_K$, with therefore more blue SPM than red one (since here $p>1$), as is indeed observed.

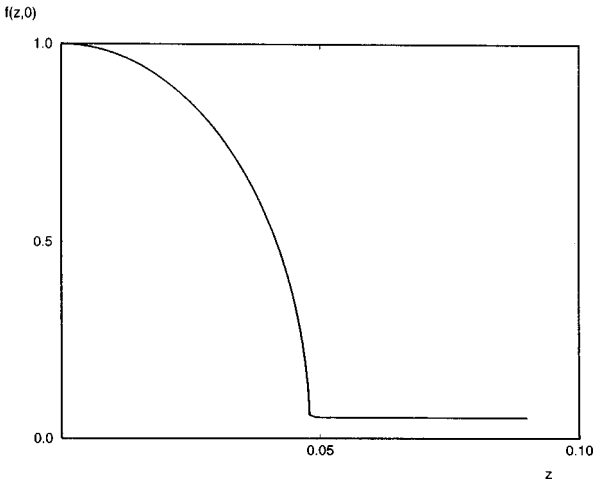

FIG. 1. Radial shrinking of the light beam normalized radius $f(z,0)$ as a function of the propagation distance z. f is taken as the time maximum of the initial pulse. z is normalized to the Rayleigh length z_r, with parameters $q^2=200$, $A=10^{-39}$, $\tau_1=\tau_2=1$, and $C=0$.

Knowing I_f, the variation of the index is found to be of the order of 2×10^{-5}, while the diffraction index, negligible at the beginning of the focusing process, reaches a value of the order of $n_d = 7\times 10^{-7}$ in the filament for $w_f = 200\,\mu$m (at $z = L_{sf}$). Thus n_d remains weak as compared to nonlinear indexes.

Also, we can justify *a posteriori* that the electron impact ionization mechanism gives an effective collision time of the order of a picosecond (the quiver energy associated with I_f is of the order of 50 eV) for full (100%) ionization and thus is negligible with respect to photoionization on the femtosecond time scale.

3. Paraxial analysis

To be complete we perform a paraxial study to compute more accurately the filament radius. We get new coupled equations for f and ϕ:

$$\partial^2_{z'^2} f(z',\zeta) = \left(1 - f^4/\tau_2 \int_{-\infty}^{\zeta} [b^2(\zeta')f^{-4}]e^{-(\zeta-\zeta')/\tau_2} d\zeta'\right) f^{-3} + pc_1^2(k_p r_i)^2 \int_{-\infty}^{\zeta} [b^{2p}(\zeta')f^{-2p-2}]d\zeta'(e^{-H_0}), \tag{46}$$

$$\partial_{z'}\varphi_{nl}(z',\zeta) = -2/f^2 + 1/\tau_2 \int_{-\infty}^{\zeta} [b^2(\zeta')/f^2]e^{-(\zeta-\zeta')/\tau_2} d\zeta' - c_1^2(k_p r_i)^2(1-e^{-H_0}), \tag{47}$$

$$H_0(z',\zeta) = c_1^2 \int_{-\infty}^{\zeta} [b^{2p}(\zeta')/f^{2p}]d\zeta'.$$

$$c_1^2 = \sigma_p I_0^p \tau, \quad k_p = c/\omega_{pn}.$$

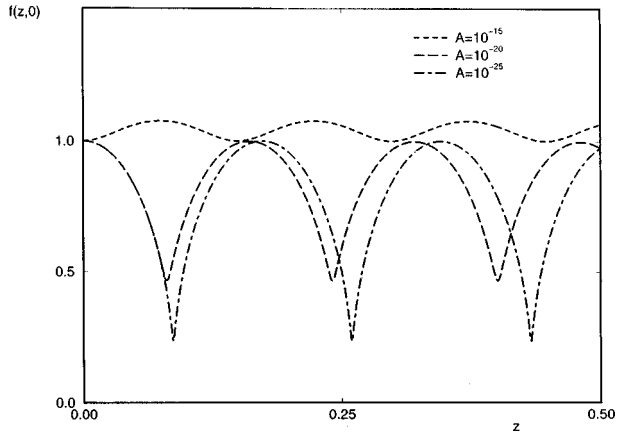

FIG. 2. Sensitivity of $f(z,0)$ as a function of the propagation distance z for various initial values of A, the same parameters as above otherwise.

The system of equations (46) and (47) has been integrated by a fourth-order Runge-Kutta method, keeping the f function in the integrals when required. We do observe the stabilization in z of the radius f to a finite value when the intensity increases thanks to the balance of the two nonlinearities. Figure 1 shows the shrinking of the radius using figures relevant for the experiments presented in [2]. The simple condition $f''=0$ gives a good estimation of the radius reduction by a factor of 100 in agreement with the experimental case. Figure 2 shows the spatial oscillations of the beam radius for different values of the initial coefficient $A=pc_1^2(k_p r_i)^2$ entering into the multiphoton ionization nonlinearity. We can notice the great sensitivity of f to the value of A.

A more thorough analysis to compute the filament size is done by writing at the filament edge $r=r_f$ the condition $dr_f/dz=0$ (see also [15]), again neglecting diffraction. This condition provides the relation

$$r_f=\lambda_d(2P_f/P_c)^{1/2}. \tag{48}$$

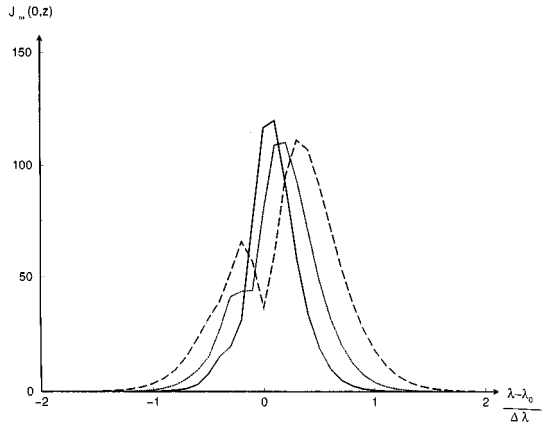

FIG. 3. Spectra $J_\omega(0,z)$ in arbitrary units of u for various z with the same parameters as in Fig. 1. In the abscissa we have plotted a normalized wavelength $(\lambda-\lambda_0)/(\Delta\lambda), \Delta\lambda=\lambda_0^2/2\pi C\tau$. (a) $z=0.01$ (solid line), (b) $z=0.02$ (dotted line), and (c) $z=0.03$ (dashed line)

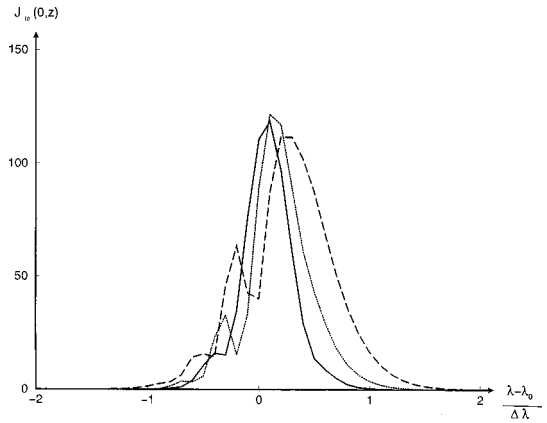

FIG. 4. Spectra $J_\omega(0,z)$ of u with the same parameters than in Fig. 3 except that $C=-1$. (a) $z=0.01$ (solid line), (b) $z=0.02$ (dotted line), and (c) $z=0.03$ (dashed line)

Diffraction would bring another unity term as compared to the power ratio in Eq. (48), as in Eq. (19) for L_{sf}. The condition (48) curiously does not determine r_f or the filament power P_f since we also have the relation

$$P_f=(\pi r_f^2 I_f). \tag{49}$$

Thus a compatibility condition is required, yielding

$$I_f=P_c/2\pi\lambda_d^2. \tag{50}$$

This last relation again gives either I_f or the ionization rate α. Using Eq. (45), we find the energy into the filament to be around 0.7–1 mJ. This is about the experimental value, allowing us to check the value of $P_f=(E_f/\tau)$. Without time compression the result is $P_f=7$ GW and $r_f=2-3\lambda_d=100-200\,\mu$m, not very far from the rough estimation (45) and in good agreement with the observations. If we have had only a mere beam radius reduction, the final power P_f' would had been only $P_f'=P_0(r_f/r_0)^2$, much weaker than P_f. Cooperative action between neighboring rays and light concentration due to the nonlinearity involved seems to exist. Also, note that P_f is only a few times P_c in the stable filaments.

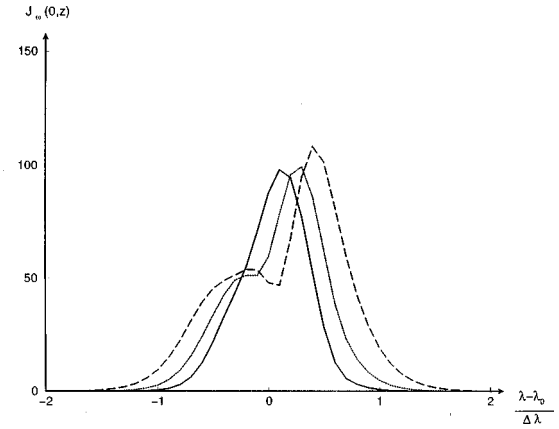

FIG. 5. Spectra $J_\omega(0,z)$ of u with the same parameters as in Fig. 3 except that $C=+1$. (a) $z=0.01$ (solid line), (b) $z=0.02$ (dotted line), and (c) $z=0.03$ (dashed line)

This could be due to spatial inhomogeneities in the initial beam that prevent a larger amount of power from collapsing, but the presence of hot spots in the initial profile could lead also to the creation of individual filaments of comparable intensity that may interact together later on. The filament is observed to be stable over more than 30 m, but it ends by disappearing due to energy ionization losses and, to a lesser extent, due to the energy it radiates; see [2,16] for more details about light conical emission by a Cherenkov effect from an antiguidelike structure.

4. Spectral analysis

Analytical analysis of spectra has been performed to describe qualitatively the observed spectral features, and this study will be published elsewhere. Here we limit ourselves to presenting results of a numerical analysis consisting of solving Eqs. (46) and (47) for the radius and phase and then computing the spectra J given by expression (3). A numerical Fourier transform of the spectra is performed, with the use of the definitions (6)–(8) for the profile u:

$$J_\omega(r,z)=\left|\int_{-\infty}^{+\infty}[u_0(\zeta)/f(z,\zeta)]e^{-(r/r_0 f)^2/2}e^{i[(\omega-\omega_0)\zeta+\varphi_{\mathrm{NL}}(z,\zeta)+(r^2/2)f_z'/f(z,\zeta)]}d\zeta\right|^2, \tag{51a}$$

$$J_\omega(0,z)=\left|\int_{-\infty}^{+\infty}[u_0(\zeta)/f(z,\zeta)]e^{i[(\omega-\omega_0)\zeta+\varphi_{\mathrm{NL}}(z,\zeta)]}d\zeta\right|^2. \tag{51b}$$

Here we restrict ourselves to the central part of the beam computing $J_\omega(0,z)$ without the need to account for radial convolution. Using the initial data profile given by Eq. (15) for u, we obtain in Figs. 3–5, respectively, the spectra at different values of z corresponding to different radius locations in Fig. 1, each one for three different values of the initial time chirp parameter C.

Figure 3 is of the no chirp case, while Figs. 4 and 5 are obtained with a finite temporal chirp. In all cases one sees an increase of the redshifting of the central peak with z and the growing of the self-phase modulation in the blue part of the spectrum as predicted and in qualitative agreement with the observations. We have checked also the increase of the central peak redshift with an increase of the parameter $y=(\tau/2\tau_2)$.

IV. CONCLUSION

In conclusion, we have given an explanation, relying on a simple analytic theory, for the formation and stable propagation of light spatially localized structures into air that are initiated by ultrashort and powerful laser pulses. These structures have been experimentally demonstrated. We have used a rather simple model capable of describing qualitatively and quantitatively the filament characteristics. Improved models have to be developed in the future to make a comparison to numerical codes [17,18], in particular to include group velocity dispersion effects (when useful) and to understand possible substructures in filaments that may be probed in finer experiments. Above all, temporal aspects of beam evolution also have to be adressed, since theory indicates pulse time splitting [19] and a possible time compression of a factor of 2 within the filament [20].

ACKNOWLEDGMENTS

T.L. acknowledges useful discussions that initiated and motivated this work and access to the experimental data of the laser-matter interaction group of the Laboratoire d'Optique Appliquée (LOA) of the Ecole Polytechnique at Palaiseau, a team led by A. Mysyrowicz with P. Curley, M. Franco, G. Grillon, R. Lange, E. Nibbering, B. Prade, and J. F. Ripoche.

[1] A. Braun, G. Korn, X. Liu, D. Du, J. Squier, and G. Mourou, Opt. Lett. **20**, 73 (1995).
[2] E. T. J. Nibbering (unpublished); E. T. J. Nibbering, M. Franco, B. S. Prade, G. Grillon, C. Le Blanc, and A. Mysyrowicz, Opt. Commun. **119**, 479 (1995).
[3] O. G. Kosareva, V. P. Kandidov, A. Brodeur, C. Y. Chien, and S. L. Chin, Opt. Lett. **22**, 1332 (1997).
[4] X. Liu and D. Umstadter, in *OSA Proceedings on Shortwavelength V: Physics with Intense Laser Pulses*, edited by M. D. Perry and P. B. Corkum (Optical Society of America, Washington, DC, 1993), Vol. 17, p. 45.
[5] A. Chiron, E. T. J. Nibbering, M. Franco, B. S. Prade, G. Grillon, C. Le Blanc, B. Lamouroux, and A. Mysyrowicz, Eur. Phys. J. D **6**, 383 (1996).
[6] A. Brodeur, C. Y. Chien, F. A. Ilkov, S. L. Chin, O. G. Kosareva, and V. P. Kandidov, Opt. Lett. **22**, 304 (1997).
[7] G. P. Agrawal, *Non Linear Fiber Optics* (Academic, New York, 1989).
[8] B. S. Prade, J. M. Schins, E. T. J. Nibbering, M. Franco, and A. Mysyrowicz, Opt. Commun. **113**, 79 (1994).
[9] J. F. Ripoche, G. Grillon, B. S. Prade, M. Franco, E. Nibbering, R. Lange, and A. Mysyrowicz, Opt. Commun. **135**, 310 (1997).
[10] R. Y. Shen, *Principles of Non Linear Optics* (Wiley, New York, 1987).
[11] M. V. Ammosov, N. B. Delone, and V. P. Krainov, Zh. Eksp. Teor. Fiz. **91**, 2008 (1986) [Sov. Phys. JETP **64**, 1191 (1986)].
[12] P. F. Curley, E. T. J. Nibbering, M. A. Franco, B. S. Prade, A. Mysyrowicz, and T. Lehner, in *Proceedings of the X Conference on Ultrafast Phenomena, San Diego, 1996* (Optical Soci-

ety of America, 1996); H. R. Lange, G. Grillon, J. F. Ripoche, M. A. Franco, B. Lamouroux, B. S. Prade, A. Mysyrowicz, E. T. J. Nibbering, and A. Chiron, Opt. Lett. **23**, 2 (1998).

[13] L. Di Menza, C. H. Bruneau, and T. Lehner, Numer. Methods Partial Differential Equations **15**, 672 (1999).

[14] A. B. Borisov *et al.*, Phys. Rev. Lett. **68**, 2309 (1992); P. Sprangle, E. Esarey, J. Krall, and A. Ting, *ibid.* **69**, 2200 (1992); A. Sullivan, H. Hamster, S. P. Gordon, R. W. Falcone, and H. Nathel, Opt. Lett. **19**, 1544 (1994); H. S. Brandi, C. Manus, G. Mainfray, and T. Lehner, Phys. Fluids B **5**, 3539 (1993); H. S. Brandi, C. Manus, G. Mainfray, G. Bonnaud, and T. Lehner, Phys. Plasmas **1**, 968 (1994).

[15] E. E. Fill, J. Opt. Soc. Am. B **11**, 2241 (1994).

[16] E. T. J. Nibbering *et al.*, Opt. Lett. **21**, 62 (1996).

[17] V. P. Kandidov *et al.*, Nonlinear Opt. **12**, 119 (1995).

[18] M. Mlejnek, E. M. Wright, and J. V. Moloney, Opt. Lett. **23**, 5 (1998); Phys. Rev. E **58**, 4903 (1998).

[19] J. E. Rothenberg, Opt. Lett. **17**, 583 (1992); **17**, 1340 (1992).

[20] A. T. Ryan and G. P. Agrawal, Opt. Lett. **20**, 309 (1995); I. P. Christov, H. C. Kapteyn, M. M. Murmane, C. P. Huang, and J. Zhou, *ibid.* **20**, 306 (1995).